Energy & Environmental Science

PAPER

View Article Online
View Journal | View Issue

Cite this: *Energy Environ. Sci.*, 2018, **11**, 354

Extremely lightweight and ultra-flexible infrared light-converting quantum dot solar cells with high power-per-weight output using a solution-processed bending durable silver nanowire-based electrode†

Xiaoliang Zhang, *[ab] Viktor A. Öberg,[b] Juan Du,[a] Jianhua Liu[a] and Erik M. J. Johansson *[b]

Received 27th September 2017,
Accepted 13th December 2017

DOI: 10.1039/c7ee02772a

rsc.li/ees

Lightweight and flexible solar cells are highly interesting materials for use in new applications, such as spacecraft, aircraft and personal pack load. PbS colloidal quantum dots (CQDs) exhibit a broad and strong light absorption spectrum covering the ultraviolet-visible-near infrared region, allowing for incorporation of very thin CQD films into solar cells with high power conversion efficiency (PCE) from solar light to electricity. Herein, we report an extremely lightweight and ultra-flexible CQD solar cell constructed on a polyethylene naphthalate substrate with a thickness of 1.3 μm. A solution-processed Ag nanowire network with excellent mechanical, optical and electrical properties was prepared as the front-electrode in the solar cell. The thickness of the complete CQD solar cell is less than 2 μm, and ~10% PCE with a weight of 6.5 g m^{-2} is achieved, resulting in a power-per-weight output of 15.2 W g^{-1}. The flexible solar cell possesses durable mechanical properties and maintains high-level photovoltaic performance under extreme deformation and after repeated compression–stretching deformation. Moreover, the flexible CQD solar cell shows impressive stability both under continuous illumination and after storage under ambient conditions. These results reveal that solution-processed CQDs are compatible with an ultra-flexible substrate for the construction of ultra-lightweight infrared light-converting CQD solar cells with possibilities for new exciting solar energy applications.

Broader context

Ultra-flexible and lightweight solar cells with high power output per weight have attracted much attention due to their high potential for utilization in applications such as spacecraft, aircraft, personal pack load and wearable electronic devices. PbS colloidal quantum dots (CQD) are promising candidates for the fabrication of flexible and lightweight solar cells due to their nanocrystal character, which enables functioning energy conversion even in the case when the solar cell is under extreme deformation. Moreover, the PbS CQD possesses the advantages of solution-processability, size-dependent optoelectronic properties and a broad light absorption spectrum covering the ultraviolet-visible-near infrared wavelength region. In this study, we report an ultra-flexible and extremely lightweight PbS CQD solar cell. The solar cell is fabricated on a 1.3 μm-thick flexible polyethylene naphthalate foil substrate and an Ag nanowire network with strong mechanical properties and a large aspect ratio and is used as a transparent and conductive front-electrode. The thickness of the full solar cell is less than 2 μm and the device gives ~10% power conversion efficiency with an extremely low weight of 6.5 g m^{-2}, resulting in a high power-per-weight output of ~15 W g^{-1}. The demonstrated CQD solar cell shows good mechanical properties and works during large compression–stretching deformation. In particular, the solar cell also exhibits promising stability both under continuous illumination and after storage under ambient conditions. These results reveal that the CQDs are very promising materials for realizing flexible, efficient and extremely lightweight solar cells that makes it possible for utilization of solar energy in many new applications.

1. Introduction

Flexible and lightweight solar cells have attracted considerable attention due to the possibility of use in interesting applications, such as spacecrafts, aircrafts, portable or wearable power supplying devices, or on curved surfaces of buildings or automobiles to supply electric power, or indoor and outdoor decorations for

[a] *School of Materials Science and Engineering, Beihang University, Beijing 100191, China*
[b] *Department of Chemistry-Ångström, Physical Chemistry, Uppsala University, 75120 Uppsala, Sweden. E-mail: xiaoliang.zhang@kemi.uu.se, erik.johansson@kemi.uu.se*

† Electronic supplementary information (ESI) available. See DOI: 10.1039/c7ee02772a

multifunctioning.[1–8] The dominating silicon-based solar cell technology is based on silicon wafers, which are brittle and rather thick. Therefore, it is difficult to use silicon-based solar cells in applications that require highly flexible and extremely lightweight solar cells. Other solar cell technologies are therefore needed for these applications. Specifically, solar cell materials with strong light absorption (which reduce the solar cell thickness) and high flexibility that can be prepared at low temperature to allow for deposition on thin plastic substrates are therefore highly interesting. Moreover, solar cells fabricated on flexible substrates with a low-temperature fabrication approach are also compatible with continuous roll-to-roll fabrication approaches with spraying or printing techniques, which makes it possible for very high throughput solar cell production and therefore lowering of the solar cell cost.[9–12] The lightweight solar cell may also decrease the energy consumption for the solar cell transportation and installation and thus, further decreasing the carbon foot-print and energy pay-back time for the solar cells. In the light of these advantages, various solar cell technologies were developed to minimize the solar cell weight and maximize the solar cell flexibility, mechanical resilience and power conversion efficiency (PCE), which are primary benefits for the flexible solar cells.[13–15] The power-per-weight (or specific weight or specific power) is a critical metric for the flexible or lightweight solar cells. As such, ultrathin organic solar cells (OSCs) and perovskite solar cells (PSCs) have been reported;[2,16,17] among them, the PSC has a power-per-weight output of 22.6 W g^{-1}. In addition, the power output during and after bending is very important for the flexible solar cells, and the mechanical stability of the materials in the solar cell is therefore essential for the utilization in applications.

PbS colloidal quantum dot (CQD) is a promising material for flexible and lightweight solar cells due to its nanocrystalline character, wide and strong light absorption spectrum covering the ultraviolet (UV)-visible-near infrared (NIR) region, solution processability and size-dependent optoelectronic properties.[18–23] The CQD film may also have specifically advantageous mechanical properties due to the possibility to change the distance between the CQDs in the film without distorting the crystal structure of the CQDs. With the advances in CQD surface chemistry, energy band engineering and device architecture optimization, rapid progress has been achieved in the past few years, aiming to improve the solar cell efficiency and stability,[24–28] and a PbS CQD solar cell with a PCE of more than 11% was obtained.[29] The state-of-the-art CQD solar cells are generally constructed by inserting a CQD solid film with a thickness of 350–450 nm between an electron transport material (ZnO or TiO_2) and a metal (Au) electrode.[30] Thus, the weight and mechanical properties of the CQD solar cells are predominantly determined by the substrate and front transparent electrode. Although the flexible CQD solar cell has been demonstrated and the device possesses high bending durable mechanical properties,[31–34] the device shows much lower efficiency than the solar cell fabricated on the traditional glass/indium tin oxide (ITO) substrate. Whether ''lightweight'' can be achieved for the CQD solar cells and whether these CQD solar cells can withstand extreme deformation have not been investigated previously.

Herein, we report an extremely lightweight and ultra-flexible CQD solar cell with a high power-per-weight output. The solar cells were fabricated on a 1.3 μm-thick flexible polyethylene naphthalate (PEN) substrate at a low temperature. The thickness of the complete solar cell is less than 2 μm and a PCE of ~10% was achieved, resulting in a power-per-weight output of 15.2 W g^{-1}. The ultra-flexible CQD solar cell shows good compression–stretching mechanical stability and maintains a high power output under the extreme compressed state. Moreover, the solar cell shows good stability both under constant illumination and on storage at ambient conditions.

2. Results

2.1. Solution-processed flexible electrode

The front electrode in the flexible solar cells generally requires high optical transmittance, low sheet resistance and good mechanical properties. ITO is commercially applied as a front electrode in many optoelectronic devices due to the high transmittance and conductivity. However, the brittle properties of ITO significantly decrease the conductivity under deformation, limiting its applications in the ultra-flexible solar cells.[35,36] Conductive polymers, such as poly(3,4-ethylenedioxythiophene)-poly(styrenesulfonate) (PEDOT:PSS),[36] and carbon materials, such as carbon nanotubes and graphene,[32,37,38] have also been investigated for use as an ITO alternative electrode for flexible solar cells. However, the conductivity or transparency of these electrodes is much lower than those of the ITO-based electrodes, which result in lower solar cell efficiency compared with that of the ITO electrode-based solar cells. Metal nanowire (NW)-based electrodes, such as Ag NWs, possess remarkable conductivity, transparency and outstanding mechanical properties. Therefore, the Ag NWs are believed to be one of the most promising electrode materials for the flexible photovoltaic or optoelectronic devices.[39–42] The performance of the metal NW-based electrode generally increases with the decrease in the diameter of the NW, while the increase in the NW length/diameter aspect ratio will reduce light scattering and decrease the resistance in the film.[43–49]

Therefore, in this study, Ag NWs with an average aspect ratio of 5000 (average diameter of ~30 nm and length of 100–200 um, Fig. S1, ESI†) were utilized as the transparent and conductive front-electrodes in the flexible CQD solar cells.

The CQD solar cell was fabricated on a flexible PEN foil with a thickness of 1.3 μm, which was adhered on a glass/polydimethylsiloxane (PDMS) supporting substrate *via* van der Waals forces for the device fabrication processes as shown in Fig. 1a. After fabrication, the solar cell was peeled away from the glass/PDMS supporting substrate. The Ag NW ink was spin-coated on the PEN foil under ambient conditions. Fig. 1b presents a photograph of a sample of glass/PDMS/PEN/Ag NWs, and it can be observed that the sample is very transparent. A photograph of an Ag NW-covered glass substrate for the hard solar cell fabrication is presented in Fig. S2 (ESI†). During the deposition of Ag NWs on the substrate, the conductivity or

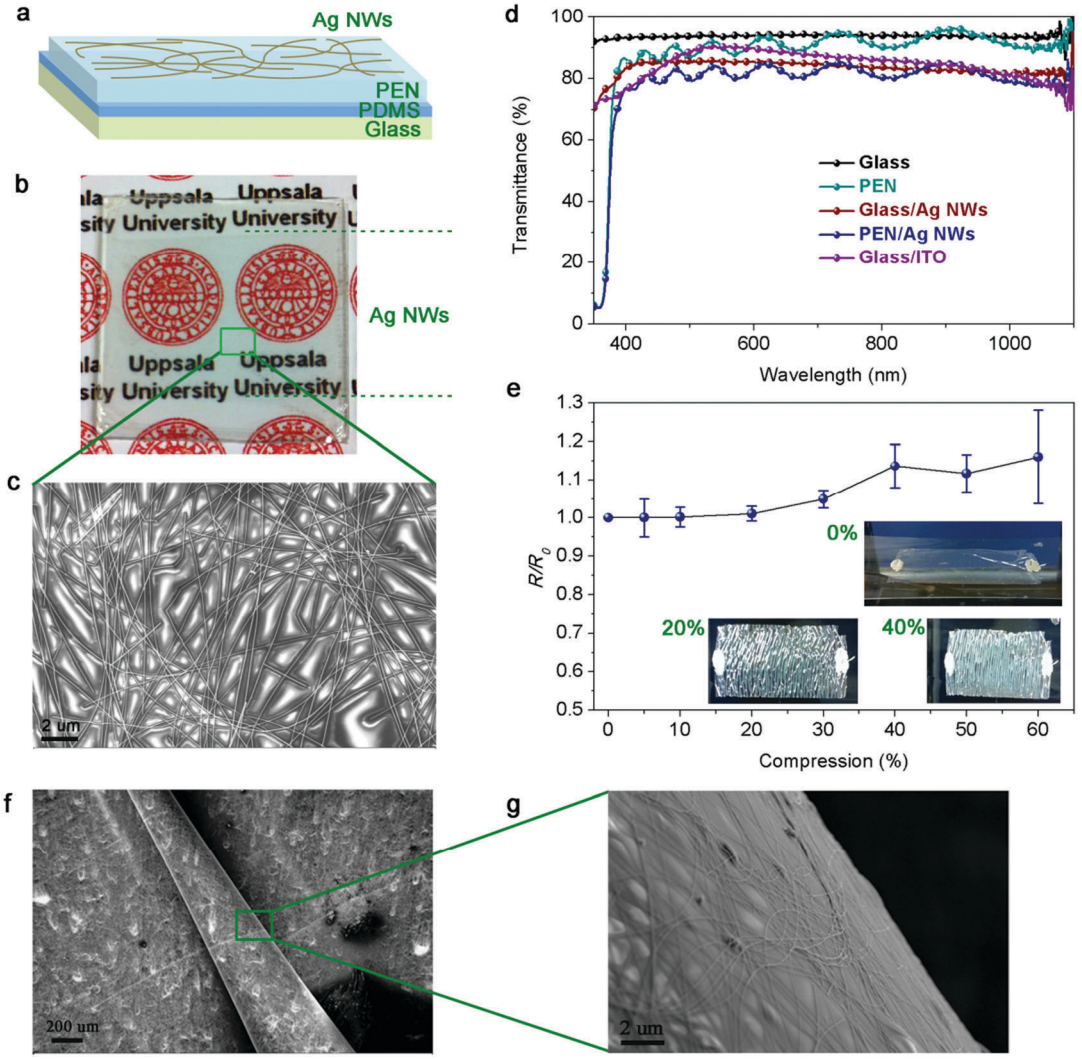

Fig. 1 Transparent and conductive Ag NW-based electrode. (a) Schematic of the Ag NW electrode preparation. The thin PEN film is adhered on the glass/PDMS supporting substrate for device fabrication. (b) Photograph of the sample of glass/PDMS/PEN/Ag NWs. (c) SEM image of the Ag NWs deposited on the PEM substrate. (d) Light transmission spectra of the Ag NWs deposited on the glass and flexible PEN substrate. (e) Resistance evolution of the Ag NW electrode under compression. Insets are photographs of the PEN/Ag NW electrode under compression state. The PEN/Ag NW network was peeled away from the glass/PDMS supporting substrate and adhered on the pre-stretched elastomer. R_0 is the resistance of the flat Ag NW electrode (0% compression), and R is the resistance of the Ag NW electrode under compression that differs (5–60%). (f) Low-magnification and (g) high-magnification SEM images of the flexible PEN/Ag NW electrode under compression. The Ag NW remains firmly adhered on the PEN substrate under the deformation without any broken NWs or NWs pointing out from the substrate.

transparency could be fine-tuned by the spin-coating (Fig. S3, ESI†). We observed that the prepared Ag NW-based electrode shows comparable or even better transparency and conductivity than the traditional ITO-based electrode, which indicates that the Ag NW electrode may offer a low-energy consumption route for high-quality electrode fabrication and may also be compatible with a solution-processed scalable roll-to-roll fabrication strategy. Fig. 1c shows a scanning electron microscopic (SEM) image of the Ag NWs deposited on the flexible PEN substrate, which reveals that an Ag NW network with contacts between the NWs is formed on the PEN substrate even though the concentration of the Ag NWs is low due to the large aspect ratio of the NWs.

Fig. 1d shows light transmission spectra of the substrate (glass and flexible PEN) and the substrate covered with the Ag NW network. For comparison, the light transmission spectra of the traditional glass/ITO substrate was also measured and plotted. It can be observed that the substrate/Ag NW network exhibits high light transmittance. In particular, the flexible PEN/Ag NW network has an average transmittance of ~80% in the visible and NIR region, which is required for the PbS CQD solar cell due to its broad light absorption spectrum. As demonstrated above, the conductivity of the transparent electrode under the deformed state is critical for the solar cell performance, directly influencing the device efficiency under deformation. To evaluate the conductivity evolution of the Ag NW networks under extreme deformation, the substrate of PEN/Ag NWs was peeled away from the glass/PDMS supporting substrate and adhered on a pre-stretched elastomer (Fig. S4, ESI†). The resistance of the

Ag NW network on the glass/PDMS/PEN and the flexible substrate PEN/Ag NWs attached on the pre-stretched elastomer was compared and we found that there is no noticeable difference in the resistance after the flexible PEN substrate is peeled away from the glass/PDMS supporting substrate (Fig. S5, ESI†). This suggests that the Ag NW network firmly sticks on the PEN substrate and shows good mechanical properties. During the separation of the flexible PEN/Ag NWs from the supporting substrate, the NW network remains is intact, thus maintaining the high-performance properties.

Fig. 1e shows the evolution of the resistance of the Ag NW network with compression; the insets are the photographs of the PEN/Ag NWs network under extreme compression. It can be observed that the Ag NW electrode maintains high conductivity even under extreme compression. The resistance of the Ag NWs network under ~60% compression increases only by ~15%, which is important for the flexible solar cell under the deformed state. Fig. 1f and g present the SEM images of the flexible PEN/Ag NW network electrode under compression, which show that the NW networks strongly adhere to the PEN substrate without any NWs broken or pointing away from the substrate.

2.2. Ultra-flexible and lightweight CQD solar cell

Fig. 2a schematically displays the solar cell device architecture with a structure of PEN/Ag NWs/AlZnO (AZO)/PbS-PbX_2 (X = I and Br)/PbS-1,2-ethanedithol (EDT)/Au. The CQD layers were prepared and deposited through solution-based methods, and the back contact Au film was deposited using thermal evaporation. The details for the solar cell fabrication are described in the Experimental section and schematically presented in Fig. S6 (ESI†). Briefly, the AZO nanoparticle (NP) layer functions as an electron transport layer in the device (Fig. S7, ESI†). The transmission spectra of the substrate covered with Ag NWs and AZO NP layer is shown in Fig. S8 (ESI†). The PbS CQD was synthesized using a hot-injection method. The light absorption and photoluminescence spectrum, and TEM image of the PbS CQDs are shown in Fig. S9 (ESI†). A bilayer of the PbS CQD solid was incorporated into the solar cell. For the first n-type PbS CQD solid layer, the CQDs were treated with PbX_2 and the second less-n type (or p-type) CQD solid layer were treated with EDT for ligand exchange. Solution-phased ligand exchange was carried out to prepare the PbS-PbX_2 CQD ink and subsequently, the PbS-PbX_2 CQD solid layer was deposited using single-step of spin-coating of the CQD ink. The CQD ink enables a flat energy landscape in the CQD solid film and shows advantages for high packing density.[29] The second CQD solid layer treated with EDT functions as an electron blocking layer in the device. The corresponding energy levels of each material are presented in Fig. 2b. The surface morphology of the AZO and CQD solid layer was measured atomic force microscopy (AFM), and the results show that the solution-processed AZO and CQD solid layers are uniform and cover a large area with low roughness (Fig. S10, ESI†). The thickness of each layer is marked in Fig. 2a; the thickness of the complete CQD solar cell is ~1.9 μm, which is around thirty times thinner than the thickness of a human hair. For comparison, a solar cell was also fabricated on the traditional glass/ITO substrate as a controlled device (Fig. S11, ESI†). Moreover, a CQD solar cell with Ag NWs on a microscopic slide as a front transparent electrode was also fabricated for comparison, and the corresponding cross-sectional SEM image is shown in Fig. S12 (ESI†).

Fig. 2c and d show the photographs of the back side and front side of the fabricated flexible CQD solar cell, respectively. The solar cell was placed on a dandelion, and it can be seen that there is no deformation of the dandelion observed (Fig. 2e), which implies that the fabricated CQD solar cell exhibits extremely light-weight properties. Fig. 2f shows the solar cell under the compression state when the solar cell was adhered on the pre-stretched elastomer. The device was uniformly wrinkled as the elastomer relaxed and this allowed for evaluation of the device performance under the compression state, which will be discussed in the following section.

The photovoltaic performance of the device was measured under the AM 1.5G 100 mW cm^{-2} illumination. Fig. 2g presents the photocurrent density–voltage (J–V) characteristic curves of the CQD solar cells fabricated on the different substrates; the corresponding photovoltaic parameters are summarized in Table 1. The solar cell constructed on the traditional glass/ITO substrate shows an open-circuit voltage (V_{oc}) of 0.65 V, a short-circuit current density (J_{sc}) of 25.7 mA cm^{-2} and a fill factor (FF) of 0.65, resulting in a high PCE of 10.8%. The Ag NW electrode-based solar cells fabricated on glass and flexible PEN substrates give an impressive PCE of 9.7% and 9.9%, respectively. During the J–V measurement, different voltage scanning directions (forward (from J_{sc} to V_{oc}) and backward (from V_{oc} to J_{sc})) as well as different voltage scanning rates were applied for the measurements. The results reveal that no hysteresis behavior was observed for the demonstrated flexible CQD solar cell and there is no noticeable effect of different voltage steps (1–100 mV) in the J–V measurements (Fig. S13 and S14, ESI†).

Fig. 2h shows the incident photon-to-current efficiency (IPCE) spectra of these solar cells. The solar cells have broad light absorption and the flexible solar cells have a relatively lower IPCE value in the UV region due to the absorption of the PEN substrate (Fig. 1d). The photocurrent density was integrated from the IPCE results, which indicate that the integrated photocurrent is in agreement with the results from the J–V measurements (Fig. S15, ESI†).

The steady-state photocurrent density (J_{MPP}) and efficiency at the maximum power point (MPP) of the flexible solar cell were tested under continuous AM 1.5G 100 mW cm^{-2} illumination (Fig. 2i). The device shows a stable J_{MPP} and a slightly increased power output within a short-term illumination of 400 s. The long-term steady-state performance is discussed further below. Fig. 2j presents the statistical analyses results of the CQD solar cells fabricated on the different substrates. The devices show high reproducibility and the CQD solar cells with Ag NW network as the front electrode have similar performance, which suggests that the demonstrated CQD solar cells are substrate insensitive, offering much room for appropriate substrate selection for certain applications.

2.3. Mechanical properties of ultra-flexible CQD solar cell

The CQD solar cell performance under extreme mechanical deformation is important for use in flexible and foldable

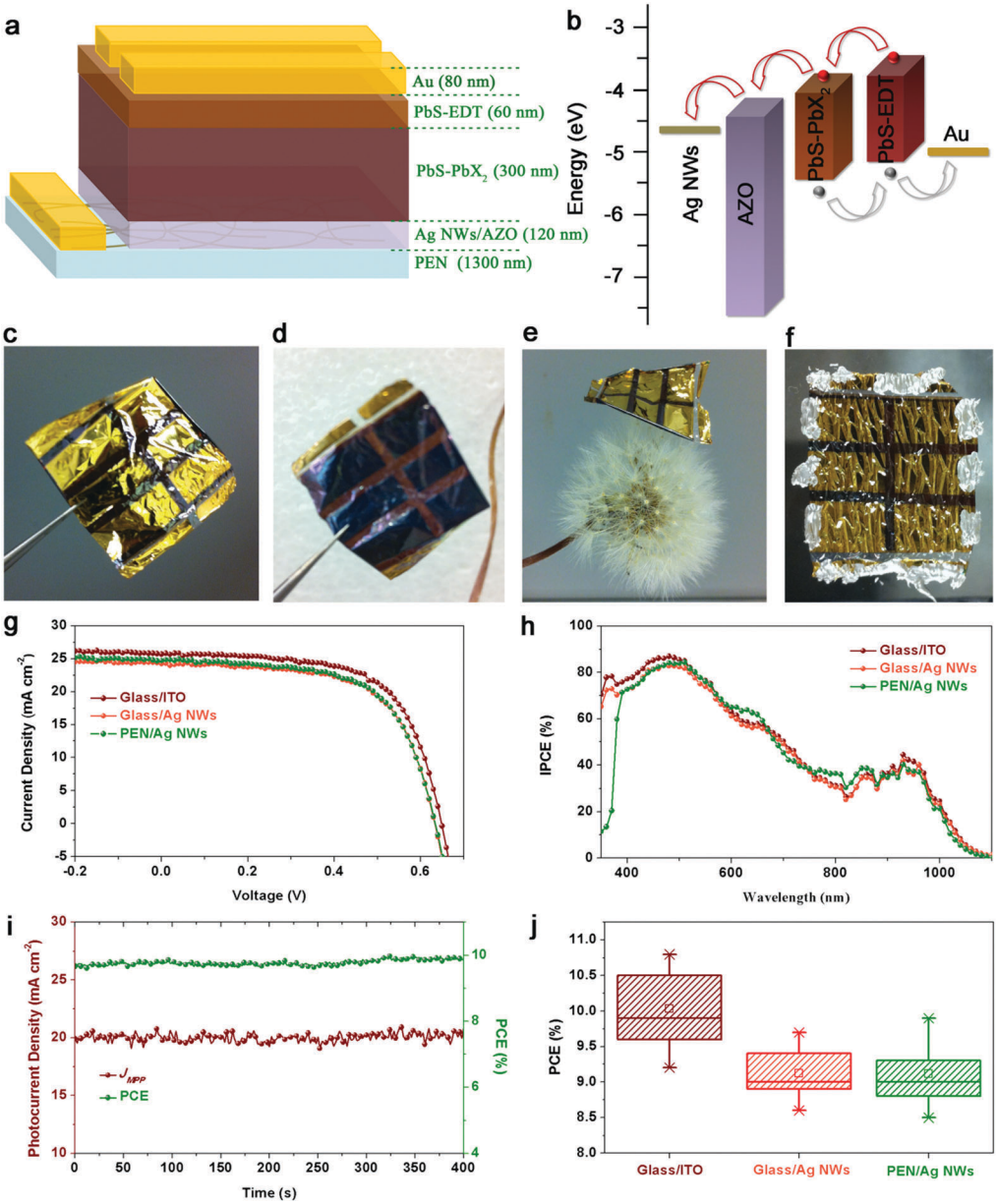

Fig. 2 Device architecture and performance of the ultra-flexible and lightweight CQD solar cell. (a) Schematic structure of the CQD solar cell with a device architecture of PEN/Ag NWs/AZO/PbS-PbX_2/PbS-EDT/Au. (b) Energy levels of the materials used for the device fabrication. The energy levels were obtained from the literature.[29,30,50] Red and gray ball presents the photoinduced electron and hole, respectively, which transport to the corresponding electrode under the built-in electric field within the device. Photograph of the (c) back side and (d) front side of the flexible solar cell. The size of the flexible substrate with six solar cells is $\sim 2 \times 2$ cm^2. (e) The flexible solar cell placed on a dandelion without any deformation of the dandelion. (f) The flexible solar cell under the extreme compression state. (g) *J–V* curve and (h) IPCE spectra of the CQD solar cell with glass/ITO, glass/Ag NWs and flexible PEN/Ag NWs substrate, respectively. The *J–V* curves were recorded under AM 1.5G 100 mW cm^{-2} illumination. (i) Steady-state efficiency and photocurrent density of the flexible solar cell at the MPP. (j) Statistics comparing the solar cells with glass/ITO, glass and PEN substrates, respectively.

Table 1 Photovoltaic performance of the CQD solar cell fabricated on the different substrates. The performance was measured under AM 1.5 G 100 mW cm^{-2} illumination

Substrate	V_{oc} (V)	J_{sc} (mA cm^{-2})	FF	PCE (%)
Glass/ITO	0.65 (0.64 ± 0.1)	25.7 (24.8 ± 0.8)	0.65 (0.64 ± 0.1)	10.8 (9.9 ± 0.9)
Glass/Ag NWs	0.64 (0.63 ± 0.1)	24.4 (23.8 ± 0.8)	0.62 (0.61 ± 0.1)	9.7 (9.1 ± 0.6)
PEN/Ag NWs	0.64 (0.63 ± 0.1)	24.6 (23.6 ± 0.9)	0.63 (0.62 ± 0.1)	9.9 (9.0 ± 0.9)

applications. Therefore, the flexible CQD solar cell was peeled away from the glass/PDMS supporter and stacked on a pre-stretched elastomer *via* van der Waals forces (Fig. S16, ESI†). The width of the elastomer is much larger than the solar cell size to assure that the strain will be nearly one dimensional and uniform on the solar cell. The elastomer was slowly relaxed and the photocurrent–voltage (*I*–*V*) curve was recorded by compression of 5 or 10% steps. During the compression, folds and winkles were uniformly formed on the solar cells and under high compression, the density of the folds and wrinkles largely increased (Fig. 3a). Fig. 3b shows the *I*–*V* curves of the flexible CQD solar cell under compression, which shows that the device maintains functional solar cell properties even under 60% compression. The corresponding IPCE spectra of the flexible CQD solar cell under compression are displayed in Fig. S17 (ESI†), which shows that the solar cell shows comparable IPCE when the solar cell is under small compression (<30%).

The photovoltaic parameters of the flexible solar cell under compression are summarized in Fig. 3c. The solar cell maintains high-level output of FF and V_{oc} under compression and almost no degradation in the V_{oc} and FF was observed until 40% compression. The photocurrent and power output (POP) nearly linearly decreases until 40% compression due to the linear decrease in light absorption area of the solar cell, leading to nearly constant PCE of ~9% accounting for the decreased surface area during compression. The SEM images of the solar cell under compression are presented in Fig. S18 (ESI†). When the flexible CQD solar cell is under high compression, cracks are observed on the Au electrode and part of the Au electrode is broken off from the solar cells, which may lead to the decreased performance (Fig. S19, ESI†).

In certain applications, it is important that the solar cell should operate even after the device is re-stretched to the flat state after the compression. Therefore, the solar cell was also

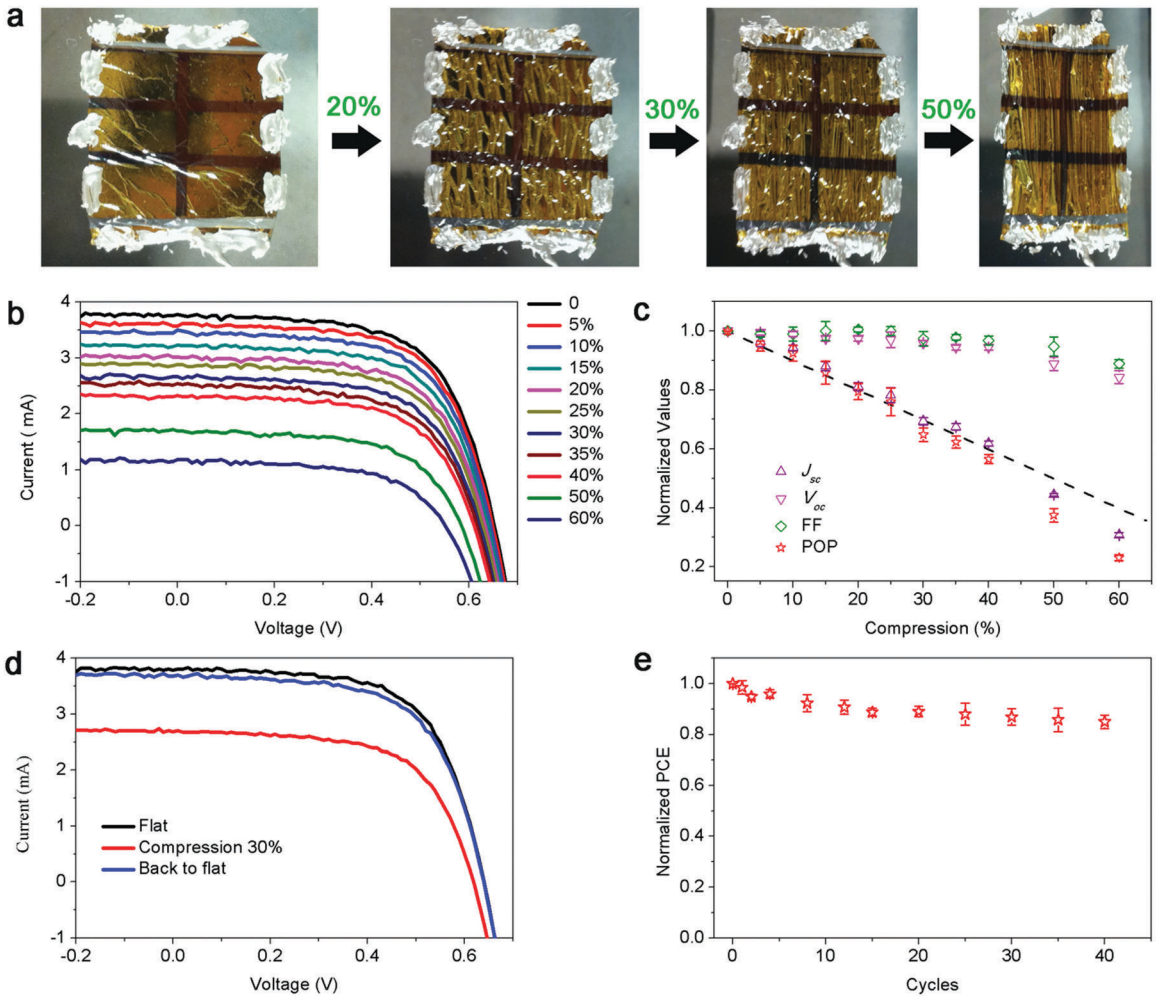

Fig. 3 Photovoltaic performance of the flexible CQD solar cell under the compression–stretching. (a) Flexible CQD solar cell was adhered on the pre-stretched elastomer. The elastomer is slowly relaxed and the compression starts from flat (0 compression) until 60% compression with steps of ~5% or ~10%. (b) *I*–*V* curves of the solar cell under linear compression. (c) Photovoltaic parameter metrics of the solar cell as a function of the compression. The solar cell gives nearly constant PCE of ~9% (without any masks for the measurement) with the compression until 40% compression. POP: power output. (d) *I*–*V* curves of the solar cell under flat state (0 compression), 30% compression and re-stretched back to flat state (0 compression). (e) Device efficiency metrics plotted at each 30% compression–stretching during 40 continuous cycles.

compressed from 0 (flat) to 30% by linear compression and re-stretched back to 0 (flat). The cyclic compression–stretching was repeated for 40 cycles and for each cyclic compression-stretching, the *I–V* curves were recorded (Fig. S20, ESI†). Fig. 3d shows the *I–V* curves of the first cyclic compression–stretching. We found that a slightly lower photocurrent was obtained after the solar cell was re-stretched to the flat state from 30% compression compared with the original photocurrent. Fig. 3e shows the device efficiency as a function of cyclic compression–stretching; the other photovoltaic parameters are summarized in Fig. S21 (ESI†). The corresponding IPCE spectra of the flexible CQD solar cell with compression–stretching cycles are displayed in Fig. S22 (ESI†). After 40 repeated compression–stretching cycles, ~85% of original performance is maintained. The slightly decreased efficiency with cyclic compression–stretching is primarily attributed to the decreased FF and V_{oc}, which may result from the increased resistance in the devices probably due to cracks in the Au electrode or due to parts of the Au electrode flakes off the solar cell. The solar cell performance under compression–stretching in parallel to the Au electrode array was also studied, which suggests that the solar cells show similar results independent of the compression–stretching direction (Fig. S23, ESI†).

2.4. Solar cell stability

The solar cell stability is critical for the flexible solar cell overall photovoltaic performance and is also important for practical applications. Therefore, the stability of the flexible CQD solar cell is tested under both continuous illumination and after

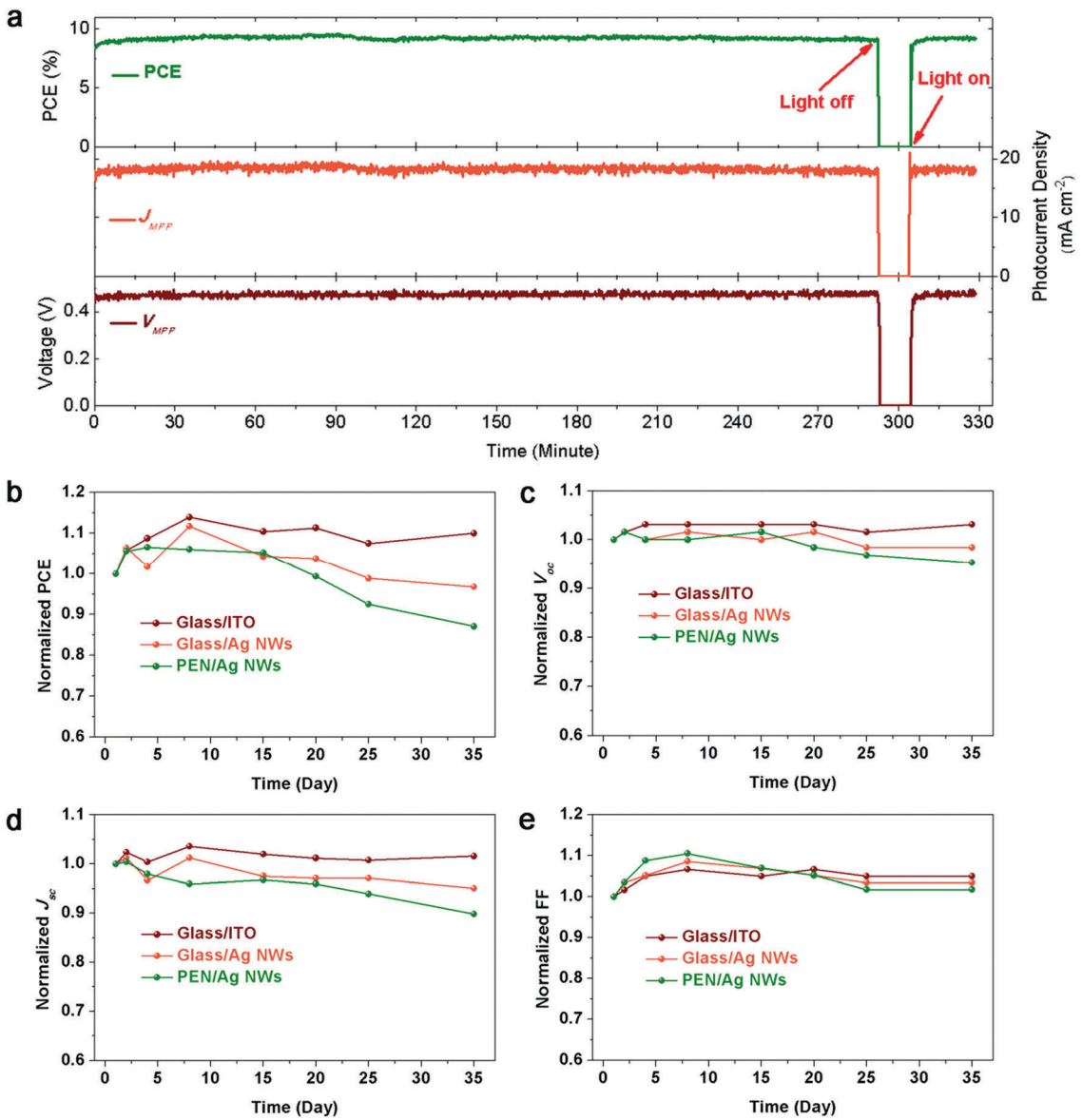

Fig. 4 Stability upon illumination and storage under ambient conditions. (a) Steady-state efficiency, photocurrent density and photovoltage of the flexible CQD solar cell at the MPP under continuous AM 1.5G 100 mW cm^{-2} illumination. Normalized (b) PCE, (c) V_{oc} (d) J_{sc} and (e) FF of the CQD solar cells fabricated on the different substrates *versus* time of storage under ambient conditions.

storage under ambient conditions. The flexible solar cell was placed under a solar simulator with continuous AM 1.5G 100 mW cm^{-2} illumination for ~290 min. The evolutions of the J_{MPP}, photovoltage (V_{MPP}) and PCE at the MPP were traced with the illumination time as shown in Fig. 4a. The flexible CQD solar cell maintains high-level output during the continuous illumination and we did not find any noticeable degradation. Both J_{MPP} and V_{MPP} maintain a high-level output, which results in that the device efficiency is almost the same as the original efficiency. During the photostability measurement, after around 290 min, the illumination was blocked using a mechanical shutter and the solar cell was placed under dark condition for ~10 min. Then, the shutter was removed and the solar cell was again subjected to the AM 1.5G 100 mW cm^{-2} illumination. The solar cell showed rapid light-response and quickly retained its previous photovoltaic performance obtained before closing the shutter.

The unencapsulated CQD solar cells with different substrates were also stored under ambient conditions. Fig. 4b–e show the evolution of the photovoltaic parameters of the CQD solar cell with storage time, which show that the solar cells maintain high-level performance. No significant degradation was observed for the glass/ITO-based solar cell after storage for 35 days; moreover, more than 85% of original efficiency was maintained for the flexible solar cell. Therefore, we conclude that the demonstrated CQD solar cells exhibit promising stability both under continuous illumination conditions and after storage under ambient conditions.

3. Discussion

High power conversion efficiency is generally highly desirable in numerous solar cell applications. However, concerning certain applications, the power output per weight (watts-per-gram) may be more important compared with the energy conversion per unit area. For application as a lightweight portable power source, in areas such as spacecraft, aircraft and personal pack load, the pay load is a premium.[2,16] For these purposes, various lightweight solar cells have been studied. Table S1 (ESI†) summarizes the watts-per-weight output of different lightweight solar cells. Traditional lightweight solar cells, such as silicon and copper indium gallium selenide (CIGS) solar cells, have a watt-per-weight output of <3.5 W g^{-1}. Recently, an ultrathin PSC, constructed on a 1.4 μm-thick PET substrate with PEDOT:PSS as a front electrode, has a PCE of 12% and weight of 5.2 g m^{-2}, leading to a power-to-weight output of 22.6 W g^{-1}.[17] The flexile CQD solar cell demonstrated in this work shows a PCE of 9.9% and 6.5 g m^{-2}, leading to a power-to-weight output of ~15.2 W g^{-1}. Due to the broad light absorption spectrum and strong light absorption of PbS CQDs, the CQD solid with a thickness of 350–450 nm is generally applied in the solar cells, which is an advantage for lightweight solar cells. Moreover, the solution-processed CQD may be an ideal material for the continuous fabrication approaches, such as roll-to-roll printing or spray techniques. This study also shows the advantage of the CQD-based solar cells regarding flexibility due to the possibility to change the distance between the CQDs during compression or stretching without affecting the material within the CQD.

The results of the lightweight and ultra-flexible CQD solar cell presented in this study were also compared with previously published academic results on the flexible QD solar cells (Table S2, ESI†), which show that the flexible CQD solar cell reported in this study exhibits the highest efficiency and highest power-to-weight output. The high performance obtained by the as-prepared CQD solar cell is partly due to the higher conductivity and transparency of the Ag NW network electrode compared with the metal mesh,[51] ultrathin metal film[33] and carbon electrode,[32] which were utilized previously. Moreover, the CQD solid prepared with CQD ink technology enables a flat energy landscape in the CQD solid film and allows to improve the passivation of the PbS CQD with PbX_2, which also contributes to the improved performance.[31] Moreover, we also compared the demonstrated CQD solar cell with other solar cells with Ag NWs as a front electrode (Table S3, ESI†); we found that the CQD solar cell also shows higher efficiency than these solar cells, which may be due to the small diameter and large aspect ratio of the NWs used in this study. The similar performance of the CQD solar cell fabricated on the glass and flexible PEN substrates with the Ag NWs as a front electrode also provides great potential for the optimization by selecting the substrate according to the applications while maintaining high power conversion efficiency.

4. Conclusions

In conclusion, ultra-flexible and extremely lightweight CQD solar cells were successfully constructed. The solution-processed flexible Ag NW network electrode shows comparable transparency and conductivity as the traditional ITO-based electrode and exhibits good mechanical properties. The solar cell shows a lightweight of 6.5 g m^{-2} and high power-per-weight output of 15.2 W g^{-1}. The ultra-flexible CQD solar cell maintains high-level photovoltaic performance under extreme deformation and shows durable performance after repeated cyclic compression–stretching. Moreover, the flexible CQD solar cell shows higher efficiency than previously reported flexible CQD solar cells. The high performance is achieved due to the advantageous properties of the Ag NW front electrode with a large aspect ratio of the Ag NWs, the energy level alignment of the different layers in the solar cell, and the solution-phase ligand exchange for the CQDs. This study reveals that CQDs have a strong potential for use in lightweight and ultra-flexible solar cells, which can have many exciting future applications.

5. Experimental

5.1. Materials

Ag NWs (~20 mg mL^{-1} in isopropanol) with a diameter of ~30 nm and a length of 100–200 μm were provided by XFNANO materials Tech Co., Ltd. The flexible PEN foil (1.3 μm thickness)

and all reagents and solvents for this study were purchased from Sigma-Aldrich and used as received.

5.2. Substrate preparation

A thin PDMS (Sylgard 184, Dow Corning) layer was prepared on the glass slide (2.5 × 2.5 cm^2). The mixed solution of base and curing agent at a weight ratio of 10 : 1 was spin-coated on the glass substrate at 3000 rpm for 30 s, and subsequently annealed at 70 °C for 1 h to obtain the solid PDMS film. The PEN foil was thoroughly stretched and adhered to the glass/PDMS supporter *via* van der Waals force that allows for the solar cell fabrication processes, such as spin-coating, annealing and metal evaporation.

5.3. Solar cell fabrication

The solar cell fabrication process is schematically presented in Fig. S6 (ESI†). The Ag NW ink was prepared by diluting the obtained Ag NW ink from ~20 mg mL^{-1} to ~5 mg mL^{-1} with isopropanol and dispersed with ultrasonic dispersion for 4.5 min. The Ag NW ink was spin-coated on the PEN film at various speeds (700–4000 rpm, see ESI,† for the resulting optical and electrical properties of the films) under ambient conditions to obtain the Ag NW network with different transparencies and resistances. Then, the substrate covered with Ag NW network was sintered at 150 °C for 20 min under nitrogen atmosphere. The AZO nanoparticle ink was prepared according to the literature.[41] The AZO nanoparticle layer was deposited on the Ag NW network using spin-coating and was subsequently sintered at 140 °C for 30 min under ambient conditions.

The PbS CQDs capped with oleic acid ligand were synthesized using a hot injection method according to a previous report.[52–55] Solution-phase ligand exchange was performed prior to the CQD solid film deposition according to the literature with modification.[29] Briefly, the CQD octane solution (~10 mg mL^{-1}) was filtered using a filter with a pore size of 0.2 μm. The CQD octane solution (5 mL) was mixed with the dimethylformamide (DMF) solution (5 mL) containing 0.11 M PbI_2 and 0.03 M $PbBr_2$ and 0.04 M ammonium acetate. The mixed solution was stirred vigorously for 5 min at room temperature for ligand exchange. After ligand exchange, the CQDs transfer to the DMF phase from the octane phase and the oleic acid ligands are left in the octane phase. The octane solution was removed using a pipette and the CQDs in DMF were washed with octane for three times to thoroughly remove residual oleic acid ligands. Then, the CQDs were precipitated by adding 5 mL toluene and collected by centrifugation. After drying for 30 min under a vacuum condition, the collected CQDs were dispersed in butylamine at a concentration of ~200 mg mL^{-1}. The PbS-PbX_2 CQD solid film was deposited using single-step spin-coating CQD butylamine ink. The spin-coating process was carried out in a nitrogen atmosphere and the CQD solid film was annealed at 50 °C for 10 min in a nitrogen dry box. Another two layers of CQD solid were treated with EDT (0.01 volume% in acetonitrile) deposited on the PbS-PbX_2 CQD solid film under a nitrogen atmosphere. The CQD octane solution (~50 mg mL^{-1}) was spin-coated on the PbS-PbX_2 CQD solid at 2500 rpm for 15 s. After storing the CQD solid film under dark condition and under ambient conditions over night, an Au film with a thickness of 80 nm was thermally evaporated on the top of the CQD solid film to complete the solar cell device. After Au deposition, the solar cell was peeled away from the glass/PDMS supporting substrate.

5.4. Characterization

The light transmission spectra were measured using an Ocean Optics HR2000 spectrometer equipped with a Micropack DH-2000-BAL light source. SEM images were measured using a scanning electron microscope (SEM, Zeiss LEO1550) at an accelerating voltage of 5 kV. TEM images were measured using a transmission electron microscope (JSM 2100) at an accelerating voltage of 200 kV. The steady-state PL spectra were recorded using the Fluorolog Spectrophotometer (HORIBA JOBIN YNON). AFM images were obtained using the DIMENION icon with ScanAsyst equipment under ambient condition. The sheet resistance of the Ag NW network electrodes was measured using a four-point probe equipment (Automatic four-point probe CMT-SR2000N).

The solar cell photovoltaic performance was measured under a Newport solar simulator (model 91160) with AM 1.5G illumination as the light source at with intensity of 100 mW cm^{-2}. The light intensity was calibrated using a certified reference Si solar cell (Fraunhofer ISE) before the measurement. The *J–V* curve was scanned using the Keithley model 2400 digital source meter under nitrogen atmosphere. The solar cells fabricated on the controlled glass/ITO and glass substrates as well as glass/PDMS supported flexible solar cells were initially measured using a black metallic mask with an area of 0.068 cm^2. The voltage sweep rate was set at 10 mV with a delay of 10 ms for the voltage sweeping. Changing the voltage sweep rate and sweep direction of the solar cell did not generate a noticeable difference in the results. IPCE spectra were measured using a computer-controlled setup consisting of a xenon lamp (Spectral Products ASBXE 175), a monochromator (Spectral Products CM110), a LabJack U6 and a potentiostat (PINE, AFRDE 5). A certified reference solar cell (Fraunhofer ISE) was used for calibration prior to measurement.

The photovoltaic performance under the compression and the cyclic compression–stretching measurements were conducted by sticking the flexile solar cell on a pre-stretched elastomer. Silver paste was placed on the overhead of Au electrode to increase the conductivity with the connection. The elastomer was slowly relaxed or stretched and the *I–V* curve was recorded using the Keithley model 2400 digital source meter under ambient conditions.

The photovoltaic performance under compression and the cyclic compression–stretching measurements were conducted by sticking the flexible solar cell on a pre-stretched elastomer. A silver paste was placed on top of the Au electrode to increase the stability of the electrical connection to the measurement cable. The elastomer was slowly relaxed or stretched and the *I–V* curve was recorded using the Keithley model 2400 digital source meter under ambient conditions.

5.5. Calculation of power-per-weight

The power-per-weight is defined as the device power output per unit area under AM 1.5G 100 mW cm^{-2} illumination to the device weight per unit area.[16,17] The flexible CQD solar cell

demonstrated in this study has a PCE of 9.9% and weight of $\sim$6.5 g m^{-2}. For 1 m^2 area and under AM 1.5G 100 mW cm^{-2} illumination, the device would therefore generate 9.9 W power output with a specific weight of 15.2 W g^{-1}. The data of other solar cells are presented in Table S1 (ESI†), which was obtained from the literatures or approximate calculation after the density of each layer in the solar cells is determined.[16,17,56–61]

Author contributions

X. Z. and E. M. J. J. designed the research and experiments. X. Z. synthesized AZO NPs and PbS CQDs. X. Z. and V. Ö. fabricated solar cells and measured the solar cell performance. X. Z. conducted the resistance, SEM images, light absorption and transmission spectra measurements. V. Ö. performed the calculation of power-per-weight. J. D. and J. L. performed the TEM and AFM measurements and analyzed the data. X. Z. wrote the manuscript and prepared the figures. All authors contributed to discussions and commented on the manuscript, and all authors reviewed the manuscript.

Conflicts of interest

There are no conflicts to declare.

Acknowledgements

This work was funded by Göran Gustafsson Foundation, Swedish Energy Agency, the Swedish Research Council FORMAS, ÅForsk, Swedish Research Council (VR) and Olle Engkvist Foundation. The authors thank Dr L. Häggman for discussion and technical support. The authors thank M. Wang and G. Boschloo for the help of photostability measurements and discussion.

References

1 S. S. Shin, W. S. Yang, J. H. Noh, J. H. Suk, N. J. Jeon, J. H. Park, J. S. Kim, W. M. Seong and S. I. Seok, *Nat. Commun.*, 2015, **6**, 7410.
2 Y. Li, L. Meng, Y. M. Yang, G. Xu, Z. Hong, Q. Chen, J. You, G. Li, Y. Yang and Y. Li, *Nat. Commun.*, 2016, **7**, 10214.
3 F. Di Giacomo, A. Fakharuddin, R. Jose and T. M. Brown, *Energy Environ. Sci.*, 2016, **9**, 3007–3035.
4 D. Yang, R. X. Yang, J. Zhang, Z. Yang, S. Z. Liu and C. Li, *Energy Environ. Sci.*, 2015, **8**, 3208–3214.
5 C. Bi, B. Chen, H. Wei, S. DeLuca and J. Huang, *Adv. Mater.*, 2017, **29**, 1605900.
6 D. J. Lipomi, B. C. Tee, M. Vosgueritchian and Z. Bao, *Adv. Mater.*, 2011, **23**, 1771–1775.
7 C. Roldán-Carmona, O. Malinkiewicz, A. Soriano, G. Mínguez Espallargas, A. Garcia, P. Reinecke, T. Kroyer, M. I. Dar, M. K. Nazeeruddin and H. J. Bolink, *Energy Environ. Sci.*, 2014, **7**, 994–997.
8 A. M. Zamarayeva, A. E. Ostfeld, M. Wang, J. K. Duey, I. Deckman, B. P. Lechene, G. Davies, D. A. Steingart and A. C. Arias, *Sci. Adv.*, 2017, **3**, e1602051.
9 Q. Wang, Y. Yu, J. Yang and J. Liu, *Adv. Mater.*, 2015, **27**, 7109–7116.
10 E. H. Sargent, *Nat. Photonics*, 2012, **6**, 133–135.
11 J. Yoon, L. Li, A. V. Semichaevsky, J. H. Ryu, H. T. Johnson, R. G. Nuzzo and J. A. Rogers, *Nat. Commun.*, 2011, **2**, 343.
12 T. Kim, J. H. Kim, T. E. Kang, C. Lee, H. Kang, M. Shin, C. Wang, B. Ma, U. Jeong, T. S. Kim and B. J. Kim, *Nat. Commun.*, 2015, **6**, 8547.
13 Y. Wang, S. Bai, L. Cheng, N. Wang, J. Wang, F. Gao and W. Huang, *Adv. Mater.*, 2016, **28**, 4532–4540.
14 S. Pan, Z. Yang, P. Chen, J. Deng, H. Li and H. Peng, *Angew. Chem., Int. Ed. Engl.*, 2014, **53**, 6110–6114.
15 Z. Zhang, X. Li, G. Guan, S. Pan, Z. Zhu, D. Ren and H. Peng, *Angew. Chem., Int. Ed. Engl.*, 2014, **53**, 11571–11574.
16 M. Kaltenbrunner, M. S. White, E. D. Glowacki, T. Sekitani, T. Someya, N. S. Sariciftci and S. Bauer, *Nat. Commun.*, 2012, **3**, 770.
17 M. Kaltenbrunner, G. Adam, E. D. Głowacki, M. Drack, R. Schwödiauer, L. Leonat, D. H. Apaydin, H. Groiss, M. C. Scharber, M. S. White, N. S. Sariciftci and S. Bauer, *Nat. Mater.*, 2015, **14**, 1032–1039.
18 M. Graetzel, R. A. Janssen, D. B. Mitzi and E. H. Sargent, *Nature*, 2012, **488**, 304–312.
19 Y. Cao, A. Stavrinadis, T. Lasanta, D. So and G. Konstantatos, *Nat. Energy*, 2016, **1**, 16035.
20 M. Yuan, M. Liu and E. H. Sargent, *Nat. Energy*, 2016, **1**, 16016.
21 G. H. Carey, A. L. Abdelhady, Z. Ning, S. M. Thon, O. M. Bakr and E. H. Sargent, *Chem. Rev.*, 2015, **115**, 12732–12763.
22 I. Moreels, Y. Justo, B. De Geyter, K. Haustraete, J. C. Martins and Z. Hens, *ACS Nano*, 2011, **5**, 2004–2012.
23 I. Moreels, K. Lambert, D. Smeets, D. De Muynck, T. Nollet, J. C. Martins, F. Vanhaecke, A. Vantomme, C. Delerue, G. Allan and Z. Hens, *ACS Nano*, 2009, **3**, 3023–3030.
24 C. H. Chuang, P. R. Brown, V. Bulovic and M. G. Bawendi, *Nat. Mater.*, 2014, **13**, 796–801.
25 X. Lan, S. Masala and E. H. Sargent, *Nat. Mater.*, 2014, **13**, 233–240.
26 M. A. Boles, D. Ling, T. Hyeon and D. V. Talapin, *Nat. Mater.*, 2016, **15**, 141–153.
27 P. R. Brown, D. Kim, R. R. Lunt, N. Zhao, M. G. Bawendi, J. C. Grossman and V. Bulovic, *ACS Nano*, 2014, **8**, 5863–5872.
28 X. Lan, O. Voznyy, A. Kiani, F. P. Garcia de Arquer, A. S. Abbas, G. H. Kim, M. Liu, Z. Yang, G. Walters, J. Xu, M. Yuan, Z. Ning, F. Fan, P. Kanjanaboos, I. Kramer, D. Zhitomirsky, P. Lee, A. Perelgut, S. Hoogland and E. H. Sargent, *Adv. Mater.*, 2016, **28**, 299–304.
29 M. Liu, O. Voznyy, R. Sabatini, F. P. Garcia de Arquer, R. Munir, A. H. Balawi, X. Lan, F. Fan, G. Walters, A. R. Kirmani, S. Hoogland, F. Laquai, A. Amassian and E. H. Sargent, *Nat. Mater.*, 2017, **16**, 258–263.
30 J. Choi, Y. Kim, J. W. Jo, J. Kim, B. Sun, G. Walters, F. P. Garcia de Arquer, R. Quintero-Bermudez, Y. Li, C. S. Tan, L. N. Quan, A. P. T. Kam, S. Hoogland, Z. Lu, O. Voznyy and E. H. Sargent, *Adv. Mater.*, 2017, **29**, 1702350.

31 I. J. Kramer, G. Moreno-Bautista, J. C. Minor, D. Kopilovic and E. H. Sargent, *Appl. Phys. Lett.*, 2014, **105**, 163902.
32 X. Zhang, K. Aitola, C. Hagglund, A. Kaskela, M. B. Johansson, K. Sveinbjornsson, E. I. Kauppinen and E. M. Johansson, *ChemSusChem*, 2017, **10**, 434–441.
33 X. Zhang and E. M. J. Johansson, *Nano Energy*, 2016, **28**, 71–77.
34 X. Zhang, J. Zhang, J. Liu and E. M. Johansson, *Nanoscale*, 2015, **7**, 11520–11524.
35 B. J. Worfolk, S. C. Andrews, S. Park, J. Reinspach, N. Liu, M. F. Toney, S. C. Mannsfeld and Z. Bao, *Proc. Natl. Acad. Sci. U. S. A.*, 2015, **112**, 14138–14143.
36 W. Zhang, B. Zhao, Z. He, X. Zhao, H. Wang, S. Yang, H. Wu and Y. Cao, *Energy Environ. Sci.*, 2013, **6**, 1956–1964.
37 D. Angmo, J. Sweelssen, R. Andriessen, Y. Galagan and F. C. Krebs, *Adv. Energy Mater.*, 2013, **3**, 1230–1237.
38 I. Jeon, T. Chiba, C. Delacou, Y. Guo, A. Kaskela, O. Reynaud, E. I. Kauppinen, S. Maruyama and Y. Matsuo, *Nano Lett.*, 2015, **15**, 6665–6671.
39 S. Ye, A. R. Rathmell, Z. Chen, I. E. Stewart and B. J. Wiley, *Adv. Mater.*, 2014, **26**, 6670–6687.
40 S. Cho, S. Kang, A. Pandya, R. Shanker, Z. Khan, Y. Lee, J. Park, S. L. Craig and H. Ko, *ACS Nano*, 2017, **11**, 4346–4357.
41 J. H. Seo, I. Hwang, H. D. Um, S. Lee, K. Lee, J. Park, H. Shin, T. H. Kwon, S. J. Kang and K. Seo, *Adv. Mater.*, 2017, **29**, 1701479.
42 J. Ahn, H. Hwang, S. Jeong and J. Moon, *Adv. Energy Mater.*, 2017, **7**, 1602751.
43 B. Li, S. R. Ye, I. E. Stewart, S. Alvarez and B. J. Wiley, *Nano Lett.*, 2015, **15**, 6722–6726.
44 M. Song, D. S. You, K. Lim, S. Park, S. Jung, C. S. Kim, D. H. Kim, D. G. Kim, J. K. Kim, J. Park, Y. C. Kang, J. Heo, S. H. Jin, J. H. Park and J. W. Kang, *Adv. Funct. Mater.*, 2013, **23**, 4177–4184.
45 G. A. dos Reis Benatto, B. Roth, M. Corazza, R. R. Sondergaard, S. A. Gevorgyan, M. Jorgensen and F. C. Krebs, *Nanoscale*, 2016, **8**, 318–326.
46 J. Y. Lee, S. T. Connor, Y. Cui and P. Peumans, *Nano Lett.*, 2008, **8**, 689–692.
47 J. Y. Lee, S. T. Connor, Y. Cui and P. Peumans, *Nano Lett.*, 2010, **10**, 1276–1279.
48 T. Tokuno, M. Nogi, M. Karakawa, J. Jiu, T. T. Nge, Y. Aso and K. Suganuma, *Nano Res.*, 2011, **4**, 1215–1222.
49 S. Kang, T. Kim, S. Cho, Y. Lee, A. Choe, B. Walker, S. J. Ko, J. Y. Kim and H. Ko, *Nano Lett.*, 2015, **15**, 7933–7942.
50 Z. Du, M. Liu, Y. Li, Y. Chen and X. Zhong, *J. Mater. Chem. A*, 2017, **5**, 5577–5584.
51 X. Liu, X. Li, Y. Li, C. Song, L. Zhu, W. Zhang, H. Q. Wang and J. Fang, *Adv. Mater.*, 2016, **28**, 7405–7412.
52 X. Zhang, Y. Justo, J. Maes, W. Walravens, J. Zhang, J. Liu, Z. Hens and E. M. J. Johansson, *J. Mater. Chem. A*, 2015, **3**, 20579–20585.
53 X. Zhang, P. K. Santra, L. Tian, M. B. Johansson, H. Rensmo and E. M. J. Johansson, *ACS Nano*, 2017, **11**, 8478–8487.
54 X. Zhang, J. Zhang, D. Phuyal, J. Du, L. Tian, V. A. Öberg, M. B. Johansson, U. B. Cappel, O. Karis, J. Liu, H. Rensmo, G. Boschloo and E. M. J. Johansson, *Adv. Energy Mater.*, 2017, 1702049.
55 A. Romeo, G. Khrypunov, F. Kurdesau, M. Arnold, D. L. Bätzner, H. Zogg and A. N. Tiwari, *Sol. Energy Mater. Sol. Cells*, 2006, **90**, 3407–3415.
56 A. Chirilă, S. Buecheler, F. Pianezzi, P. Bloesch, C. Gretener, A. R. Uhl, C. Fella, L. Kranz, J. Perrenoud, S. Seyrling, R. Verma, S. Nishiwaki, Y. E. Romanyuk, G. Bilger and A. N. Tiwari, *Nat. Mater.*, 2011, **10**, 857–861.
57 T. Söderström, F.-J. Haug, V. Terrazzoni-Daudrix and C. Ballif, *J. Appl. Phys.*, 2008, **103**, 114509.
58 J. Zhao, A. Wang, M. A. Green and F. Ferrazza, *J. Appl. Phys.*, 1998, **73**, 1991–1993.
59 J. Zhao, A. Wang, P. Altermatt and M. A. Green, *Appl. Phys. Lett.*, 1995, **66**, 3636–3638.
60 P. Jackson, D. Hariskos, E. Lotter, S. Paetel, R. Wuerz, R. Menner, W. Wischmann and M. Powalla, *Prog. Photovoltaics*, 2011, **19**, 894–897.
61 M. A. Green, Y. Hishikawa, W. Warta, E. D. Dunlop, D. H. Levi, J. Hohl-Ebinger and A. W. Y. Ho-Baillie, *Prog. Photovoltaics*, 2017, **25**, 668–676.

